OFFICE OF NAVAL RESEARCH

Contract N00014-88-K-0482, Mod/Amend P00001

R&T Code 413h008---01

Technical Report No. 1

Preparation and Electrochemical Characterization of Conical and Hemispherical Ultramicroelectrodes

by

Reginald M. Penner, Michael J. Heben, and Nathan S. Lewis

Prepared for Publication

in

Analytical Chemistry

California Institute of Technology
Department of Chemistry
Pasadena, California 91125

October 28, 1988

CERTIFICATION OF TECHNICAL DATA CONFORMITY

The Contractor, Nathan S. Lewis hereby certifies that, to the best of his knowledge and belief, the technical data delivered herewith under Contract No. N00014-88-K-0482, Mod/Amend P00001/R&T Code 413h008---01 is complete, accurate, and complies with all requirements of the contract.

Date October 28, 1988

Name and Title of Certifying Official Nathan S. Lewis, Associate Professor of Chemistry.

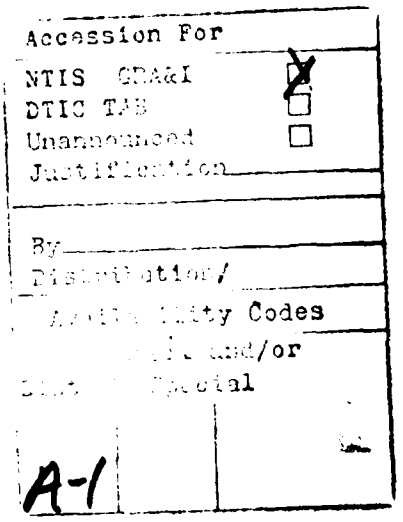

SECURITY CLASSIFICATION OF THIS PAGE

ADA201869

REPORT DOCUMENTATION PAGE

1a REPORT SECURITY CLASSIFICATION Unclassified	1b RESTRICTIVE MARKINGS
2a SECURITY CLASSIFICATION AUTHORITY	3 DISTRIBUTION / AVAILABILITY OF REPORT Approved for Public Release and Sal Distribution Unlimited
2b DECLASSIFICATION / DOWNGRADING SCHEDULE	
4 PERFORMING ORGANIZATION REPORT NUMBER(S) ONR Technical Report #1	5 MONITORING ORGANIZATION REPORT NUMBER(S)
6a NAME OF PERFORMING ORGANIZATION Nathan S. Lewis Caltech 6b OFFICE SYMBOL (If applicable)	7a NAME OF MONITORING ORGANIZATION
6c ADDRESS (City, State, and ZIP Code) M.S. 127-72 California Institute of Technology Pasadena, California 91125	7b ADDRESS (City, State, and ZIP Code)
8a NAME OF FUNDING / SPONSORING ORGANIZATION Office of Naval Research 8b OFFICE SYMBOL (If applicable)	9 PROCUREMENT INSTRUMENT IDENTIFICATION NUMBER N00014-88-K-0482/R&T 413h008---01
8c ADDRESS (City, State, and ZIP Code) Attention: Code 413 800 N. Quincy Street Arlington, VA 22217	10 SOURCE OF FUNDING NUMBERS PROGRAM ELEMENT NO / PROJECT NO / TASK NO / WORK UNIT ACCESSION NO

11 TITLE (Include Security Classification)
Preparation and Electrochemical Characterization of Conical and Hemispheric Ultramicroelectrodes

12 PERSONAL AUTHOR(S)
Penner, R.M., Heben, M. J., and Lewis, N. S.

13a TYPE OF REPORT	13b TIME COVERED	14 DATE OF REPORT (Year, Month, Day)	15 PAGE COUNT
Technical	FROM Sept 88 TO Aug 89	1988, October 28	32

16 SUPPLEMENTARY NOTATION

17 COSATI CODES		
FIELD	GROUP	SUB-GROUP

18 SUBJECT TERMS (Continue on reverse if necessary and identify by block number)
Conical, and Hemispherical Ultramicroelectrodes
Construction, and Characterization. (mgm)

19 ABSTRACT (Continue on reverse if necessary and identify by block number)

We describe a new ultramicroelectrode fabrication technique which has allowed the preparation of conical and hemispherical Pt or Ir ultramicroelectrodes with radii of 0.5 μm-10 μm. These electrodes have been characterized by scanning electron microscopy, cyclic voltammetry and chronoamperometry. The smallest radii electrodes ($r < 2$ μm) exhibited diffusional behavior in accord with a hemispherical geometry, while larger radii electrodes exhibited conical diffusion behavior. A first order mathematical approach to diffusion at conical surfaces has been developed to explain the results for these electrodes.

20 DISTRIBUTION / AVAILABILITY OF ABSTRACT	21 ABSTRACT SECURITY CLASSIFICATION
☒ UNCLASSIFIED/UNLIMITED ☐ SAME AS RPT ☐ DTIC USERS	Unclassified
22a NAME OF RESPONSIBLE INDIVIDUAL	22b TELEPHONE (Include Area Code) / 22c OFFICE SYMBOL

DD FORM 1473, 84 MAR 83 APR edition may be used until exhausted
All other editions are obsolete

SECURITY CLASSIFICATION OF THIS PAGE

PREPARATION AND ELECTROCHEMICAL CHARACTERIZATION OF CONICAL AND HEMISPHERICAL ULTRAMICROELECTRODES

Reginald M. Penner, Michael J. Heben, and Nathan S. Lewis*

Contribution #7861

Division of Chemistry and Chemical Engineering

California Institute of Technology

Pasadena, CA 91125

ABSTRACT: We describe a new ultramicroelectrode fabrication technique which has allowed the preparation of conical and hemispherical Pt-Ir ultramicroelectrodes with radii of 0.5 μm-10 μm. These electrodes have been characterized by scanning electron microscopy, cyclic voltammetry and chronoamperometry. The smallest radii electrodes ($r < 2$ μm) exhibited diffusional behavior in accord with a hemispherical geometry, while larger radii electrodes exhibited conical diffusion behavior. A first order mathematical approach to diffusion at conical surfaces has been developed to explain the results for these electrodes.

*Author to whom correspondence should be addressed.

INTRODUCTION

The construction of Pt, Au and graphite ultramicrodisk electrodes with element radii as small as 0.1 μm has become routine in many electrochemical laboratories (1). The inherently small RC time constants of ultramicroelectrodes (UMEs) allow fast, transient electrochemical experiments to be performed (2), and the low total current allows voltammetry to be performed in highly resistive media (3). Additionally, mass transport to a UME is extremely rapid, and this permits the determination of very high heterogeneous rate constants using steady-state voltammetry (4). However, the interpretation of steady-state electrochemical results for the disk geometry is complicated by the fact that the steady-state current density near the edge of a microdisk is much greater than at the center of the disk (4d,5). Consequently, the mathematical analysis of cyclic voltammetry and chronoamperometry at microdisks is complicated, and frequently involves approximations (2,5,6).

UMEs possessing a hemispherical geometry would circumvent this problem, since the steady-state current density at a hemispherical surface is uniform. Consequently, simplified mathematical treatments are available for this electrode geometry (7). Unfortunately, conventional UME construction techniques are not well suited to preparing hemispherical ultramicroelectrodes (1). Thus, experimental results for this UME geometry, despite its obvious theoretical advantages, are notably absent from the literature.

We report here a new procedure for preparing both glass and polymer insulated Pt-Ir UMEs. These UMEs can be fabricated with either conical or hemispherical geometries, and cone-hemisphere radii of 0.5 μm-10 μm are routinely accessible. We also present data for the electrochemical characterization of these electrodes by cyclic voltammetry and chronoamperometry. The chronoamperometry data for conical UME's has been analyzed in terms of a combined linear diffusion and radial diffusion expression, and these measurements have yielded the first experimental information on the diffusional properties of cone shaped microelectrodes.

EXPERIMENTAL

I. **Chemicals**. Reagent grade $K_4Fe(CN)_6$, KCl, KOH, and Na_2SO_4 (all from J.T. Baker) and NaCN (Mallinckrodt) were used as received. Aqueous solutions were prepared using 18 MΩ-cm deionized

water obtained from a Bronsted Nanopure system. Poly-(α-methylstyrene) (Aldrich, MW = 60,000) was used as received. Pt(70%)-Ir(30%) wire (dia. = 0.020") was obtained from Englehard Industries.

II. Apparatus.

A. Electrochemistry. Chronoamperometry and cyclic voltammetry were performed using a Princeton Applied Research (PAR) Model 173 potentiostat in conjunction with a PAR Model 175 voltage programmer. Cyclic voltammograms at scan rates below 500 mV s^{-1} were recorded on a Houston Instruments Model 2000 X-Y recorder. Data from faster voltammetric sweeps, or from current-time transients, were recorded on a Nicolet Model 2090 III digital storage oscilloscope. DC currents were measured using a Keithley Model 427 Current Amplifier, and AC currents were measured with a Keithley Model 177 Voltmeter. Etching characteristics were recorded using a Linear Co. strip chart recorder.

Electrochemical cells were of a conventional one-compartment design. All microelectrode experiments were performed using a conventional three-electrode configuration and a saturated calomel reference electrode.

B. Scanning Electron Microscopy. Scanning electron microscopy and energy dispersive x-ray (EDX) elemental analysis was performed with a CamScan SEM equipped with a Tracor-Northern x-ray analyzer and data station. A typical accelerating voltage for these measurements was 20 kV. Prior to SEM examination, all electrodes were coated with ca. 200 Å of gold using a plasma coater.

III. Tip Etching. The electrochemical etching bath consisted of an unstirred solution of 2 M NaOH and 6 M KCN. The cyanide facilitated the complexation and dissolution of metal from the immersed wire, and the NaOH inhibited the formation of HCN. All etching was performed in a fume hood.

To manipulate the sample during etching, the Pt-Ir wire (1.5-2.0 cm in length) to be etched was mounted in a chuck which had an adjustable distance travel. A 3" inner diameter wax-impregnated graphite ring was used as the counter electrode, and this ring was centered around the Pt-Ir tip. The Pt-Ir wire and C counter electrode were then lowered simultaneously into the etching bath until approximately 1 mm of the Pt-Ir wire was in the solution. An AC voltage of 25 V RMS was applied between the two electrodes, and the depth of immersion was adjusted until the current was 1.25 A RMS.

Etching was terminated when the desired conical geometry and aspect ratio was obtained (see **RESULTS**, section I).

IV. Tip Coating

A. Glass Coating Procedures. A coating apparatus was constructed in order to apply controllable, uniform coatings of non-porous glass insulation to the etched Pt-Ir tips. The apparatus, depicted in Figure 1, consisted of a tip positioner that facilitated variable speed tip translation and of a filament that produced molten glass beads to coat the tip.

The glass was maintained at the desired temperature by a resistively-heated ($T \leq 1700$ °C) 0.020" Pt filament. In order to localize molten glass beads by surface tension, part of the filament was bent into a tear-drop shape that measured approximately 1.5 mm in inner diameter. To provide for measurement of the filament's temperature, 0.005" Pt and Pt-Rh(10%) thermocouple wires were welded to the Pt filament.

The filament was supported by two brass posts that were fed through a plexiglass base. The brass posts were cooled by water that flowed through the posts. These posts also provided electrical contact to the filament. Prior to melting the glass, the entire filament-post system was covered with a bell jar and was evacuated through a port in the plexiglass base.

A soda-lime glass (Corning Glass #0080) was chosen for tip coating because its thermal expansion coefficient closely matched that of Pt(70%)-Ir(30%) (8). Additionally, the low viscosity of the soda-lime glass at temperatures readily accessible with a Pt filament (8) was an important property. Prior to use, the glass was cleaned with i-C_3H_7OH and deionized water.

To prepare the glass for coating the metal tip, a section of a 2 mm diameter glass rod was fed into the tear-drop of the electrically heated filament (≈ 1400 °C). The molten glass remained in the tear-drop due to surface tension. The filament was then cooled to room temperature and the system was enclosed with the bell jar and evacuated. When the interior pressure reached 40 mtorr, the filament was electrically heated to 1450 ± 20 °C for 5 minutes. During this time period, trapped gases were evolved from the molten glass bead. While maintaining a constant filament temperature, the bell jar was then vented to atmospheric pressure. This step served to insure that unescaped gas bubbles collapsed to a

size that did not introduce pinholes in the coating of the tip. The temperature of the glass was then reduced to a value used for the actual coating process, typically 1350±20 °C.

The freshly etched tip was then mounted in a collet (Figure 1), and positioners were used to center the tip relative to the molten glass bead. A manual micrometer drive then advanced the tip in the Z direction into the glass. Tip speeds between 0.05 and 5 mm/min were maintained as the tip was introduced into, and translated through, the tear-drop of molten glass. During this process, glass was transferred from the tear-drop to the tip. The electric heating current was frequently adjusted to maintain a constant filament temperature despite the changing thermal mass of the filament. The progress of the coating was monitored by observing the filament from above during the coating process. In all cases, virtually all the glass was removed from the filament with 5 to 7 mm of tip translation. Further translation exposed a portion of the bare shaft, which was subsequently gripped with tweezers in order to remove the tip from the collet.

At tip speeds greater than ≈1 mm/min, the tip was not coated, but rather the glass bead was pushed out of the tear drop by the advancing tip. At tip speeds between 0.5-1.0 mm/min, unbroken and electrically insulating glass films were obtained. Using this range of translation speeds, we have prepared tips that can be used for atomic resolution STM imaging of electrode surfaces in electrolytes containing high concentrations of redox species (9). Tip speeds between 0.3-0.5 mm/min allowed the tip to punch through the molten glass bead, and exposed small, well defined metal areas. Tip coating speeds in this interval were used to prepare the glass coated UME's described here.

B. Polymer Coating Procedures. After surveying a number of other polymers, poly(α-methylstyrene) was selected as the preferred polymer coating material. The other materials investigated either yielded erratic coating qualities (*e.g.* poly(vinylchloride)) or yielded a brittle coating that shattered during hardening (*e.g.*, polystyrene). PαMS has similar mechanical properties to polystyrene, but it has a lower T_m (10), which apparently makes it more suitable for the tip coating process. The PαMS obtained from Aldrich consisted of small polymer beads (weight = ca. 20 mg), each of which was approximately the correct size for coating a single Pt-Ir tip.

The procedure used for polymer coating was qualitatively similar to that for glass coating. Because of the lower temperatures involved in the polymer coating process, and the lack of the need to remove bubbles from the PαMS melt, a simpler polymer coating apparatus was sometimes substituted for that shown in Figure 1. This simpler apparatus consisted of a soldering iron (Ungar, 22W) onto which an "omega" shaped wire (dia. = 4 mm) was attached. The polymer bead was then supported by this wire and heated by the soldering iron.

The coating of etched Pt-Ir wires was accomplished by translating (by hand) the etched tip through the polymer melt. A typical tip translation speed was approximately 0.5 mm/sec, although qualitatively similar UME tip behavior was observed for tip speeds between 0.25 and 1.0 mm/sec. In contrast to the glass coating process, the rate of tip translation during the polymer coating step did not appear to be an important variable in determining the final coating morphology.

The quantity of exposed metal at the coated tip was found to vary reproducibly with the polymer melt temperature. The polymer temperature was monitored by immersion of an iron-constantan thermocouple wire directly into the melt. During coating, the polymer melt was adjusted to a temperature of 190-205 ^{o}C. Within this temperature range, the diameter of the cone-hemisphere radius of the coated tip decreased from 10 μm to 0.5 μm as the temperature was increased. At slightly higher temperatures (205-215 ^{o}C), fully electrically insulated tips were obtained. A detailed description of both glass and polymer insulated tips, emphasizing the capabilities of these types of electrodes with respect to electrochemical scanning tunneling microscopy, is presented in a separate publication (9).

V. Electrochemical Pretreatment and Surface Conductivity. Following glass or polymer coating, reversible steady-state voltammograms in the $Fe(CN)_6^{4-}$ test solution were not always observed initially. Instead, for approximately 10% of the UMEs with either type of insulation, the cyclic voltammetry appeared to be quasi-reversible, with plots of $log[(i_T-i)/i]$ *vs.* $E-E_{1/2}$ yielding slopes of 80-90 mV (4f). However, when such electrodes were potentiostatted at -0.6 V *vs.* SCE for several minutes, the apparent reversibility of the $Fe(CN)_6^{4-/3-}$ wave usually improved. Slopes of $log[(i_T-i)/i]$ *vs.* $E-E_{1/2}$ were then close to 60 mV, as expected for reversible electron transfer processes (4f). This observation suggests that a surface oxide layer was initially present at the exposed Pt-Ir surface, and was possibly

introduced during the preceding electrochemical etch. Electrochemical reduction of this oxide then enabled routine voltammetry to be performed with these UME's.

An additional complication was sometimes observed with glass-coated UME's. In some cases, the cyclic voltammetry of $Fe(CN)_6^{4-/3-}$ was superimposed on steeply sloping background currents. This observation suggested the presence of a parallel resistance in the electrochemical equivalent circuit. This current was found to result from a surface conductivity effect. Insulating the exposed metal shaft of such electrodes with epoxy was found to remove the sloping background component from these voltammograms, and resulted in normal, reversible electrochemical behavior.

RESULTS

I. Properties of Etched Pt-Ir Tips

The coating of Pt-Ir metal tips by glass and polymer layers was found to be a function of the sharpness, surface roughness, and cone angle of the etched tips. Extremely sharp metal tips (tip radius < ca. 1 μm) facilitated the polymer and glass coating processes, and these tips resulted in the conical UME geometries of interest to this study. Consequently, as a crucial starting point to tip preparation, the etching characteristics of 0.020" Pt(70%)-Ir(30%) wire were investigated.

Figure 2a shows a representative *i vs.* t curve for tip etching with a 25V AC rms voltage in the KCN-KOH bath. Two distinct regions, with an abrupt transition, may be discerned in the Figure. In Stage I, visual inspection of the tip indicated that the diameter of the immersed portion of the tip was uniformly reduced with etching time, while the length remained essentially unchanged. After approximately 300 sec, an abrupt transition to Stage II appeared in the i-t profile. This also corresponded to a dramatic change in the etching mechanism of the tip. During this second stage the long and narrow metal filament that resulted from Stage I etching was reduced in length without further reduction in diameter. The shapes of tips emersed at points labelled "A" or "B" in Figure 2a are schematically represented in the corresponding portions of Figure 2b. A tip removed 5 seconds after the abrupt transition from Stage I to Stage II etching, symbolized in the portion of Figure 2b labelled "stop", was repeatably found to be morphologically smooth and sharp, with an aspect ratio (α) of

approximately 1.2-1.3 (height/base diameter). These tips were well suited for subsequent coating by either polymer or glass.

An SEM image of a typical etched (but uncoated) Pt-Ir tip is shown in Figure 3. The geometry of this tip was close to conical, with an aspect ratio $\alpha \approx 1.3$ and an ultimate tip radius of 0.5 μm. Using the etching procedure described above, this geometry was obtained reproducibly, and tip radii of 0.5-1.0 μm were readily obtained.

The surface of the hemispherical tip was observed to be smooth to the limiting resolution of the SEM. This indicates that the metal underwent an effective electropolishing process during etching (11). For this reason, further polishing of the metal surface, even after insulating with glass or polymer coatings, was not necessary. Also, the longitudinal grooves revealed by the SEM images of the tip shaft were not detrimental to the final UME perfor .ance characteristics, because this area was insulated from contact with the electrolyte by the glass/polymer coating process.

Over a variety of runs, we observed that etched tips varied widely in geometry and morphology as a result of changes in etching voltage, etching time, or the age of the etching solution. Fortunately, the current *vs.* time relationships of the tips provided a bath-independent means by which the etching process could be monitored. Such curves reliably described the evolution of the tip structure for most experiments, and the above etching procedure was found to be quite satisfactory for producing the desired tip features. Additionally, varying the termination time of the etching process yielded "sharp" tips possessing aspect ratios from 0.5 to 10. Although we have found that an aspect ratio of 1.2-1.4 is optimal for obtaining polymer and glass coated UME's, the etching procedure is thus capable of producing other types of tips, if desired, for use in other applications.

II. Characterization of Insulated UME Tips

A. Scanning Electron Microscopy. Figure 4 displays SEM images of representative etched and coated Pt-Ir microelectrodes. In the glass coated UME shown in Figure 4a, the interface between the glass insulator and the exposed metal surface is clearly visible. Notably, although this interface is neither geometrically uniform nor concentric with the conical tip geometry, no cracks or other defects in the glass-metal seal are evident. In SEM images of polymer coated UMEs, such as that shown in Figure

4b, a well defined interface was not apparent between the polymer insulator and the exposed metal surface. The difficulty in resolving this interface implies that there was an intimate seal between these two components of the UME. Defects, cracks and other mechanical deformations were similarly absent in SEM images of other glass-coated and polymer-coated UMEs. Thus, it appears that both the glass and polymer coatings adhere extremely well to the etched Pt-Ir surface. This feature is critical for making well-defined microelectrodes using any tip insulation process.

The exact location of the insulator-metal boundry for polymer coated tips was determined using both SEM imaging and EDX spectroscopy. The increased brightness near the apex of the polymer coated tip in the SEM image of Figure 4b is consistent with the expected increase in electron backscattering efficiency at exposed Pt-Ir regions. This conclusion was corroborated by obtaining EDX spectra as a function of position along the tip axis. Selected spots (0.05 μm x 0.05 μm) at a series of distances from the tip apex were analyzed for the presence of Pt. Pt absorption lines were clearly evident at the areas near the tip apex. However, the intensity of these absorptions decreased as the electron beam traversed the interface between the bright and dark regions of the SEM image (Figure 4b). At distances greater than 0.5 μm beyond this interface, Pt absorption lines were no longer discernable, supporting the conclusion that the dark regions in the SEM image corresponded to coated areas of the metal wire.

The exposed metal surface of the polymer coated UME (Figure 4b) closely approximated a conical geometry, with an aspect ratio (α = 1.2) similar to that of the etched, uncoated Pt-Ir tips (Figure 3). In addition, no significant texture of the metal surface is apparent in the SEM image of Figure 4b, indicating that the surface was smooth on a scale of 0.1 μm. Greater roughness is visible at the exposed metal tip of the glass-coated UME (Figure 4a). This indicates that the characteristic conical tip geometry produced by the etching procedure described above is not retained after exposure of the metal to the high temperatures inherent to the glass coating procedure.

B. Cyclic Voltammetry. Cyclic voltammograms for representative glass-coated and polymer-coated UMEs in aqueous 4.34 m$\underline{M}$ $Fe(CN)_6^{4-}$, 1.0 $\underline{M}$ KCl solutions are shown in Figure 5a and 5b, respectively. At the two slowest scan rates (2 and 10 mV/sec) in this Figure, the shape of the voltammograms are

sigmoidal, and no cathodic wave was observed. The combination of these two features indicates that radial diffusion was established and that steady-state mass transport conditions were present for both types of tips (12). At faster scan rates (50, 200, 1000 mV sec^{-1}), significant forward and reverse peak currents were observed, indicating the presence of diffusional mass transport limitations on these timescales (12).

These data can be used to estimate the critical (or smallest) dimension of the exposed metal at the UME tip. As a first approximation, steady-state diffusion current to the conical electrode geometry indicated by the SEM images of Figure 4 can be estimated from the hemispherical diffusion equation. This implies that the radii of these UMEs can be estimated from the limiting current, i_l, using the equation describing hemispherical diffusion: $i_l = 2\pi nFDCr$ (7). The limiting currents obtained from the 2 mV/sec scans in Figure 4 are $i_{l,glass}$ = 7.1 nA, and $i_{l,polm.}$ = 16.4 nA. These values yield hemispherical radii of 3.4 μm and 7.85 μm for the glass and polymer coated UME's respectively.

An independent estimate of the small dimension of the exposed metal surface is available from the change in the shape of the cyclic voltammogram as a function of scan rate. The appearance of peaks (both cathodic and anodic) in the voltammogram signals the onset of linear diffusion. This condition occurs when the diffusion layer thickness becomes much less than the smallest dimension of the electrode (12). Thus, an analysis of the voltammetry in the transition region between linear and spherical diffusion yields an estimate of the UME radius which is independent of that calculated using the value of the limiting current. A quantitative treatment of linear scan voltammetry at microdisk electrodes by Aoki *et. al.* (5f) has shown that a unique relationship exists between the dimensionless parameter, $p = (nFr^2\nu/RTD)^{1/2}$ (where r = electrode radius, ν = voltage scan rate) and the ratio between the voltammetric peak current and the steady state limiting current, i_p/i_l. The values of this ratio for the 1 V/sec scans shown in Figure 5 are 1.1 and 1.3, respectively. These values are consistent with electrode radii of 2 μm for the glass coated UME (Figure 5a) and 7 μm for the polymer coated UME (Figure 5b)(5f), which are in reasonable agreement with the radii calculated from the limiting current formula for hemispherical diffusion.

The position of the insulator-metal interface obtained from the SEM images and EDX data yielded cone radii of 8.2 μm for the polymer-coated UME and 2.8 μm for the glass-coated UME. These values are compared in Table I with those obtained from cyclic voltammetry. Since voltammetric radius values were calculated using the hemispherical limiting current equation (*vide supra*), the agreement shown in Table I suggests that this equation is an acceptable approximation to the steady-state electrochemical behavior of these cone shaped UMEs. The particularly close agreement evident in Table I for the polymer coated UME and the precise conical geometry evident in SEM images of these electrodes provided the basis for the selection of polymer coated UMEs for the chronoamperometric experiments described below.

C. Chronoamperometry. A quantitative evaluation of the electrochemical behavior of these ultramicroelectrodes is possible using chronoamperometry (6). Figure 6a shows typical i *vs.* $t^{-1/2}$ data in aqueous 0.5 M Na_2SO_4- 4.21 mM $Fe(CN)_6^{4-}$ solutions for polymer-coated UMEs possessing radii of 1.7, 4.8, and 6.5 μm (as estimated from the observed i_l values for these electrodes). In these experiments, the potential was stepped from 0.0 V to 0.5 V *vs.* SCE. Note that the linearity of these plots is excellent (correlation coefficient > 0.99) for times between 60 μsec and 0.1 sec.

Because the concentration of ferrocyanide in this solution and its diffusion coefficient (7.94×10^{-6} cm^2/sec (6a)) are known, the slopes of these plots can be used in the Cottrell equation to calculate an apparent electrode area. These areas are listed in Table II.

The i *vs.* $t^{-1/2}$ data at long times (t > 0.1 sec) are shown in greater detail in Figure 6b. Positive deviations of the experimental data from the Cottrell line are particularly evident for the 4.8 μm and 6.5 μm radii UME's. These positive deviations are expected in the time interval where a transition from linear diffusion to hemispherical diffusion is occurring (6). This change in the mode of diffusion will occur when the diffusion layer increases in thickness and assumes dimensions greater than those of the conical metal surface (12). Thus, a quantitative analysis of the i *vs.* t data in this transition region should yield information regarding the size and the geometry of the exposed metal at the UME tip.

A first order mathematical description of the chronoamperometric transients for a general electrode geometry can be obtained by writing the total diffusion limited current as a sum of the planar flux and radial flux diffusion components:

$$i_{total} = i_{planar} + i_{radial} \qquad (1).$$

The form of the planar component of this expression is given by the well known Cottrell Equation (5c,5f,6,13):

$$i_{planar} = nFAD^{1/2}C/(\pi^{1/2}t^{1/2}) \qquad (2).$$

This portion of the total current can be calculated for any electrode geometry, and will provide an excellent approximation to the total diffusion limited current at sufficiently short electrolysis times. For the particular UME geometries of interest in this work, the hemispherical area is given simply by $A_{hemi}=2\pi r^2$, while the conical area, A_{cone}, equals $\pi r_c(h^2 + r_c^2)^{1/2}$, where h and r_c are equal to the height and base radius of a right circular cone.

The geometric information of interest is contained in the radial diffusion term of Equation (1). For all UME geometries explored to date (spherical, hemispherical and disk), a general expression for the radial component in Equation (1) has been found to be (5c):

$$i_{radial} = arnFDC \qquad (3),$$

where r is the electrode radius, and a is a function of the electrode geometry (5c). For spheres $a=4\pi$, for hemispheres $a=2\pi$, and for disks a is time dependent but approaches $a=4$ as $t \rightarrow \infty$. To date, the applicability of this treatment and the appropriate value of a are unknown for conical electrodes, because the conical UME geometry has not been available for investigation.

Thus, if Equation (1) provides a correct description of the diffusion limited current response of a conical UME, the only adjustable parameter in the fitting of the chronoamperometric data in Figure 6 is the value of *a*. To apply Equation (1) to this UME geometry, the Cottrell area of the UME was obtained from the slopes of the i vs. $t^{-1/2}$ data at times < 0.1 sec. using Eq. (2). An aspect ratio of 1.2, obtained from the SEM data for the polymer-coated UMEs (*vide supra*), was then used to calculate a value for r_c, the base radius of the cone. Fitting the entire chronoamperogram to Equations (1) and (3) then yielded a best value for *a*.

Figure 7 displays experimental and theoretical log i *vs.* log t plots for the three UMEs used in the chronoamperometry of Figure 6. Only the UMEs with the two largest radii yielded chronoamperometry that deviated from hemispherical diffusion predictions; thus, only these electrodes yielded values for r_c and *a* (Table II) using the conical diffusion treatment described above. For the two conical UMEs, the agreement between the two values for *a* is excellent. Furthermore, measurement of numerous other conical UMEs in this radius range yielded *a* values of 1.9π - 2.2π. This value is close to that for the hemispherical electrode geometry, $a_{hemi} = 2\pi$ (13).

Another method for determining the value of *a* is to utilize the relationship between the steady state limiting current in the cyclic voltammetry (Figure 4) and the conical base radius r_c as determined by SEM. For steady state diffusion, Equation (3) should describe the relationship between r_c and the total observed current at the UME. For the polymer coated conical UME of Figure 4b, using the value for r_c determined by SEM analysis (8.2 μm) and the observed i_l value at 2 mV/sec (i_l = 16.4 nA) yields a value for *a* of 1.9π. This value is in excellent agreement with those determined by analysis of the chronoamperometry data using Equation (1). This implies that the semiquantitative approach of Equation (1) is a quite satisfactory description of the diffusional behavior of these conical UMEs over a range of radii and time regimes.

Also shown in Figure 7 are log i *vs.* log t calculations for these UMEs based on a hemispherical electrode geometry. The values employed for r_c were those obtained using Equation (2) and the known cone aspect ratio (α=1.2) to fit the short time chronoamperometric response, but the chronoamperometric response for the entire time regime was then calculated for diffusion to a

hemisphere of radius $r=r_c$ using Equation (1) and $a=2\pi$ in Equation (3). Note that for the 4.8 μm and 6.5 μm radii UMEs, the currents calculated by this method overlay the experimental data in the steady-state time regime, but underestimate the current values in the short time (Cottrell) regime. For example, the 6.5 μm UME has a Cottrell region which is displaced by 0.1 = log 1.25 from the hemispherical calculation. This disparity indicates that the actual electroactive surface area of the UME is 25% greater than that expected based on the steady state limiting current and a hemispherical geometry (6,7). This observation is qualitatively that expected if the exposed metal at these UME's has a conical rather than a hemispherical geometry. For a right circular cone (base radius, r_c= 6.5 μm), the aspect ratio consistent with the experimental Cottrell area is 1.20. Similarly, the conical aspect ratio corresponding to the Cottrell area of the 4.8 μm UME is α = 1.19. These values, summarized in Table II, agree well with the α values of 1.2-1.3 obtained by SEM and support the use of a value for α of 1.2 in calculating i vs. t transients using the conical model above.

The electrochemical behavior of the 1.7 μm radius UME (Figure 7c) is distinctly different from that of the larger radii UMEs discussed above. Note that the calculated log i *vs.* log t data for the hemispherical model overlays the experimental data over the entire time regime investigated. Thus, the electrochemical behavior of this electrode with respect to chronoamperometry is essentially indistinguishable from that of a hemispherical UME over the full range of experimental times (6,7). Significantly, UMEs that exhibited hemispherical diffusion behavior always possessed radii < 2 μm.

For both the 4.8 and the 6.5 μm radii UMEs of Figure 7, the current calculated from Equation (1) is in good (but not perfect) agreement with the data over the entire experimental time interval. The slight overestimate of the actual current in the transition region indicates that the value for *a* is too large in this time interval. This observation is evidence for an *a* coefficient which is weakly time dependent over this time regime. A similar situation has been observed for chronoamperometry at microdisk electrode surfaces (5c,6). Observation of a time-dependent *a* is equivalent to stating that the first order treatment given by Equation (1) is not a rigorously correct solution to the diffusion equations in this time regime. However, a rigorous solution to the diffusion equation for a cone is expected to be quite

complicated, and the semiquantitative approach embodied by Equations (1)-(3) is quite satisfactory for describing the behavior of our UMEs over the time regimes of usual experimental interest.

DISCUSSION

The combination of SEM images, cyclic voltammetric data, and chronoamperometry indicate that the tip etching/coating process is capable of producing well-defined conical and hemispherical ultramicroelectrode tip geometries. The larger radii UMEs exhibited electrochemical behavior in accord with a diffusion to a cone, and the aspect ratio and base cone radius of these electrodes given by the SEM analysis was consistent the electrochemical behavior of these tips. In contrast, for smaller radii UMEs ($r < 2\ \mu m$), chronoamperometric data at both short and long times was consistent with a hemispherical exposed metal tip geometry. Although hemispherical mercury microelectrodes have been reported previously (14), the fabrication procedure reported here is the first to our knowledge to yield solid metal electrodes in this theoretically advantageous geometry (1,14).

Assuming that the UMEs share a common etched tip geometry, a unified picture, Scheme I, can be obtained for the effects of the tip coating process. When the radius of the exposed metal approaches the ultimate etched tip radius ($r < 2\ \mu m$), the geometry of the exposed metal should approximate that of a hemisphere. Greater UME diameters should display greater amounts of lateral surface area on the conical tip surface. As shown in Table I, this behavior is in accord with the data for the UMEs examined in this work. The 1.7 μm radius electrodes exhibited a chronoamperometric response in accord with that expected for a hemispherical electrode over the entire experimental time range, while significant deviations from hemispherical behavior were observed for the 4.8 μm and 6.5 μm radii UMEs.

Our two step fabrication procedure is conceptually simple and is similar to procedures used previously to prepare glass/Pt potentiometric indicator microelectrodes for neurophysiology applications (15). However, both the etching and coating steps of the procedure have undergone significant refinement, in order that geometrically well-defined and microscopically smooth metal surfaces are exposed after insulator coating. In addition, previous workers have found it necessary to

subject the coated and etched metal wire to an intentional "exposure step", in which the insulating material is apparently removed from the coated assembly to expose bare metal (15). We have found that this step is unnecessary, because exposed metal areas with the desired geometries, and intimate insulator-metal seals, are present in coated wires prepared by our etching/coating process.

UMEs with radii both larger and smaller than those described above could be obtained by manipulating the coating conditions as described in the experimental section above. The smallest UME radius obtained using the fabrication methods described here was 0.05 μm (estimated from the voltammetric limiting current). It was routinely possible to prepare UMEs with somewhat larger radii of 0.2-0.5 μm using either the glass or polymer coating procedures. These values are comparable to the smallest electrode radii accessible using conventional microdisk construction techniques (1).

This new UME design possesses a number of other significant features: 1) no mechanical pretreatment (*i.e.*, polishing) of the UME is required (because the etched metal surface is microscopically smooth), 2) the metal-insulator seals of these electrodes are reproducible and abrupt, and 3) the procedure does not require the handling of micron size wire that is commonly used in conventional microdisk fabrication processes. Polymer coated versions of these UMEs can be prepared with a minimum of equipment in any electrochemical laboratory.

A possible disadvantage of this design is the fact that the metal surface of the UMEs described here cannot be renewed by polishing. This problem is inherent to the protruding hemispherical geometry, but is partially offset by the ease with which new UMEs can be prepared using our procedure.

An obvious application of our UME tips is in scanning tunneling microscopy. This application requires sharp, geometrically well defined tips fabricated from chemically inert conductors. Our insulated Pt-Ir tips would seem to be especially well suited to *in situ* STM applications, where faradaic currents from the body of the metal wire normally preclude effective feedback control of the tunneling current (16,17). These tips could also be used in high speed electroanalytical methods where the advantageous geometry and low total exposed surface area can be exploited. Neurophysiological studies with implanted electrodes might also benefit from easily prepared microelectrodes made of

inert metals. Applications of this tip fabrication procedure to these problems is currently being explored, and will be described in future publications.

Acknowledgments: We acknowledge the Office of Naval Research, grant #N00014-88-K-0482, for support of the research and NSL acknowledges additional support as a Camille and Henry Dreyfus Foundation Teacher-Scholar program.

Literature Cited

(1) A recent review of microelectrode construction techniques can be found in: Fleischmann, M.; Pons, S.; Rolison, D.R.; Schmidt, P.P. *"Ultramicroelectrodes"*, Datatech Systems, Inc. Morganton, NC, 1987; Chapter 3.

(2) a. Andrieux, P.; Garreau, D.; Hapiot, P.; Pinson, J.; Saveant, J.M. *J. Electroanal. Chem.* **1988**, *243*, 321. b. Wipf, D.O.; Kristensen, E.W.; Deakin, M.R.; Wightman, R.M. *Anal. Chem.* **1988**, *60*, 306. c. Andrieux, C.P.; Garreau, D.; Hapiot, P.; Saveant, J.M. *J. Electroanal. Chem.*, **1988**, *248*, 447.

(3). a. Bond, A.M.; Fleischmann, M.; Robinson, J. *J. Electroanal. Chem.* **1984**, *168*, 299. b. Bond, A.M.; Fleischmann, M.; Robinson, J. *J. Electroanal. Chem.* **1984**, *180*, 257. c. Cassidy, J.; Khoo, S.B.; Pons, S.; Fleischmann, M. *J. Phys. Chem.* **1985**, *89*, 5537. d. Howell, J.O.; Wightman, R.M. *Anal. Chem.* **1984**, *56*, 524. e. Dribble, T.; Bandyopadhyay, S.; Ghoroghchian, J.; Smith, J.J.; Sarfarazi, F.; Fleischmann, M.; Pons, S. *J. Phys. Chem.* **1986**, *90*, 5275. f. Bruckenstein, S. *Anal. Chem.* **1987**, *59*, 2098.

(4) a. Dayton, M.A.; Ewing, A.G.; Wightman, R.M. *Anal. Chem.* **1980**, *52*, 2392. b. Scharifker, B.; Hills, G. *J. Electroanal. Chem.* **1981**, *130*, 81. c. Russell, A.; Repka, K.; Dibble, T.; Ghoroghchian, J.; Smith, J. J.; Fleischmann, M.; Pitt, C.H.; Pons, S. *Anal. Chem.* **1986**, *58*, 2961. d. Bond, A.M., Oldham, K. B.; Zoski, C. G. *J. Electroanal. Chem.* **1988**, *245*, 71. e. Oldham, K.B.; Zoski, C.G.; Bond, A. M.; Sweigart, D.A. *J. Electroanal. Chem.* **1988**, *248*, 467. f. Galus, Z.; Golas, J.; Osteryoung, J. *J. Phys. Chem.* **1988**, *92*, 1103.

(5) a. Soos, Z.G.; Lingane, P.J. *J. Phys. Chem.* **1964**, *68*, 3821. b. Flanagan, J.B.; Marcoux, L. *J. Phys. Chem.* **1973**, *77*, 1051. c. Dayton, M.A.; Brown, J.C.; Stutts, K.J.; Wightman, R.M. *Anal. Chem.* **1980**, *52*, 946. d. Oldham, K.B. *J. Electroanal. Chem.* **1981**, *122*, 1. e. Galus, Z; Schenk, J.O.; Adams, R.N. *J. Electroanal. Chem.* **1982**, *135*, 1. f. Aoki, K.; Osteryoung, J., *J. Electroanal. Chem.* **1981**, *122*, 19. g.

Aoki, K.; Osteryoung, J. *J. Electroanal. Chem.* **1981**, *125*, 315. h. Shoup, D.; Szabo, A. *J. Electroanal. Chem.* **1982**, *140*, 237. j. Aoki, K.; Akimoto, K.; Tokuda, H.; Osteryoung, J. *J. Electroanal. Chem.* **1984**, *171*, 219. k. Pons, S.; Fleischmann, M. *Anal. Chem.* **1987**, *59*, 1391A.

(6) a. Hepel, T.: Osteryoung, J. *J. Phys. Chem.* **1982**, *86*, 1406. b. Hepel, T.; Plot, W.; Osteryoung, J. *J. Phys. Chem.* **1983**, *87*, 1278.

(7) Galus, Z. *Fundamentals of Electrochemical Analysis*, Halsted Press: New York, NY, 1976.

(8) Bansal, N.P.; Doremus, R.H. *Handbook of Glass Properties*, Academic Press: Orlando, FL, 1986.

(9) Heben, M.J.; Dovek, M.M.; Lewis, N.S.; Penner, R.M.; Quate, C.F. *J. Microscopy*, in press.

(10) a. *"Aldrich Handbook of Fine Chemicals"*, Aldrich Chemical Company, Milwaukee, WI, 1988. b. *"Polymer Handbook"*, Interscience: New York, NY, 1966.

(11) Petzow, G. *"Metallographic Etching"*, American Society for Metals: Metals Park, OH, 1978; Chapter 1.

(12) Wightman, R. M. *Anal. Chem.* **1981** *53*, 1125A.

(13) Delahay, P. *"New Instrumental Methods in Electrochemistry"*, Interscience: New York, NY, 1954; p. 54.

(14) a. Lines, R.; Parker V.D. *Acta Chemica Scand.* **1977**, *B31*, 369. b. Wehmeyer, R. K.; Wightman, R.M. *Anal. Chem.* **1985**, *57*, 1989. c. Golas, J.; Osteryoung, J. *Anal. Chem. Acta* **1986**, *186*, 1. d. Golas,

J.; Osteryoung, J. *Anal. Chem. Acta* **1986**, *181*, 211. e. Golas, J.; Galus, Z.; Osteryoung, J. *Anal. Chem.* **1987**, *59*, 389.

(15) a. Wolbarsht, M.L.; MacNichol, E.F., Jr.; Wagner, H.G. *Science*, **1960**, *132*, 1309. b. Guld, C. *Med. Electron. Biol. Engng.* **1964**, *2*, 317.

(16) a. Sonnenfeld, R.; Hansma, P.K. *Science* **1986**, *232*, 211. b. Itaya, K.; Sugawara, S. *Chem. Lett.* **1987**, 1927.

(17) Dovek, M.M.; Heben, M.J.; Lewis, N.S.; Penner, R.M.; Quate, C.F. *Molecular Phenomena at Electrode Surfaces*, ACS Symposium Series, in press.

Table I. Comparison of UME Radii Determined From SEM Data and Cyclic Voltammetric Data For Typical Glass and Polymer Coated UME's.

Electrode	r_{SEM} (μm)[a]	r_l (μm)[b]	r_{CV} (μm)[c]
glass	2.8	3.40	2
polymer	8.2	7.85	7

[a]Radius at the base of the exposed metal surface as estimated from SEM's shown in Figure 4.

[b]Radius calculated from the voltammetric limiting current at ν = 2 mV/sec using the expression for steady state hemispherical diffusion, $i_l = 2\pi FDCr$ (7).

[c]Radius estimated from the ratio i_p/i_l at ν = 1 V/sec using a microdisk voltammetric model (5f).

Table II. Summary of Geometric Data For Polymer Coated UME's Obtained From Chronoamperometry Experiments.

A_{expt} (cm^2)[a]	r_c (μm)	*a*	$\frac{A_{expt}}{A_{hemi}}$[f]	α[g]
3.46×10^{-6}	6.51[b]	2.000[d]	1.29	1.19
1.91×10^{-6}	4.84[b]	2.002[d]	1.30	1.20
1.81×10^{-7}	1.70[c]	2.000[e]	1.00	-

[a]Areas calculated from the slopes of the i vs. $t^{-1/2}$ plots (Figure 6a) using the Cottrell Eq. (Eq. 2).

[b]Base radius of the right circular cone with aspect ratio, α, =1.2, which possesses the Cottrell area listed in column 1. (Calculated using the equation $A = \pi r_c(r_c + h_c)^{1/2}$).

[c]Radius of the hemisphere which possesses the Cottrell area listed in column 1.

[d]Value of the *a* coefficient obtained by fitting the experimental log i vs. log t data (Figure 7) with the conical model (Eqs. 1-3) in the steady-state time regime. Values for the radius are listed in column 2 and α=1.2 is assumed.

[e]Value of the *a* coefficient from the hemispherical diffusion model.

[f]Ratio between the experimentally determined Cottrell areas for each UME listed in column 1 and the surface area of a hemisphere possessing the radius listed in column 2.

[g]Aspect ratio, α = cone height/cone diameter, of a right circular cone possessing a surface area equal the experimentally determined value and a radius calculated from the limiting current at each UME using the hemispherical diffusion equation (Eq. (3), $a = 2\pi$).

Figure Captions

Figure 1 - Schematic diagram of the apparatus used to apply glass or polymer layers to etched Pt-Ir wires. A complete description is found in the text.

Figure 2 - Current vs. time curve for a 0.020" Pt-Ir wire etched in an unstirred aqueous solution containing 6 M NaCN and 2 M KOH. The etching voltage was 25 V RMS. Schematic representations of tips emersed at the points labeled "A", "B", and "STOP" are shown in the lower half of the Figure.

Figure 3 - Scanning electron micrograph (SEM) of the tip of a Pt-Ir wire after electrochemical etching.

Figure 4 - a. SEM image of the glass coated UME used to obtain the cyclic voltammetry data shown in Figure 5a. b. SEM image of the polymer coated UME used to obtain the cyclic voltammetry data shown in Figure 5b.

Figure 5 - a. Cyclic voltammograms for a typical glass coated UME immersed in 4.34 mM $Fe(CN)_6^{4-}$, 1 M KCL (Aq.) at potential scan rates of: a. = 2 mV/sec, b. = 10 mV/sec, c. = 50 mV/sec, d. = 200 mV/sec, e. = 1000 mV/sec. b. Cyclic voltammograms for a typical polymer coated UME in the same solution. Scan rates are the same as in Figure 5a.

Figure 6 - Current vs. $time^{-1/2}$ plots for potential steps at three polymer coated, Pt-Ir UMEs. Potential steps were applied from 0.0 V to 0.5 V vs. SCE in 4.21 mM $Fe(CN)_6^{4-}$, 0.5 M Na_2SO_4 (Aq.). o = 6.5 μm radius UME, Δ = 4.8 μm radius UME, = 1.7 μm radius UME. a. Data for time interval from 60 μsec to 3 sec. b. Data for time interval from 35 msec to 3 sec.

Figure 7 - Comparison of experimental Log i vs. Log t plots for the data of Figure 6 with that calculated for both the conical electrode geometry (solid line) and the hemispherical electrode geometry (broken line). The calculations were done using Equations 1-3, as described in the text. o = 6.5 μm radius UME, Δ = 4.8 μm radius UME, = 1.7 μm radius UME.

Scheme I - Representation of the etched tip geometry showing the approximate location of the insulator-metal interface (broken lines) for the 1.7 μm, 4.8 μm, and the 6.5 μm radii polymer coated UMEs examined in the chronoamperometry section.

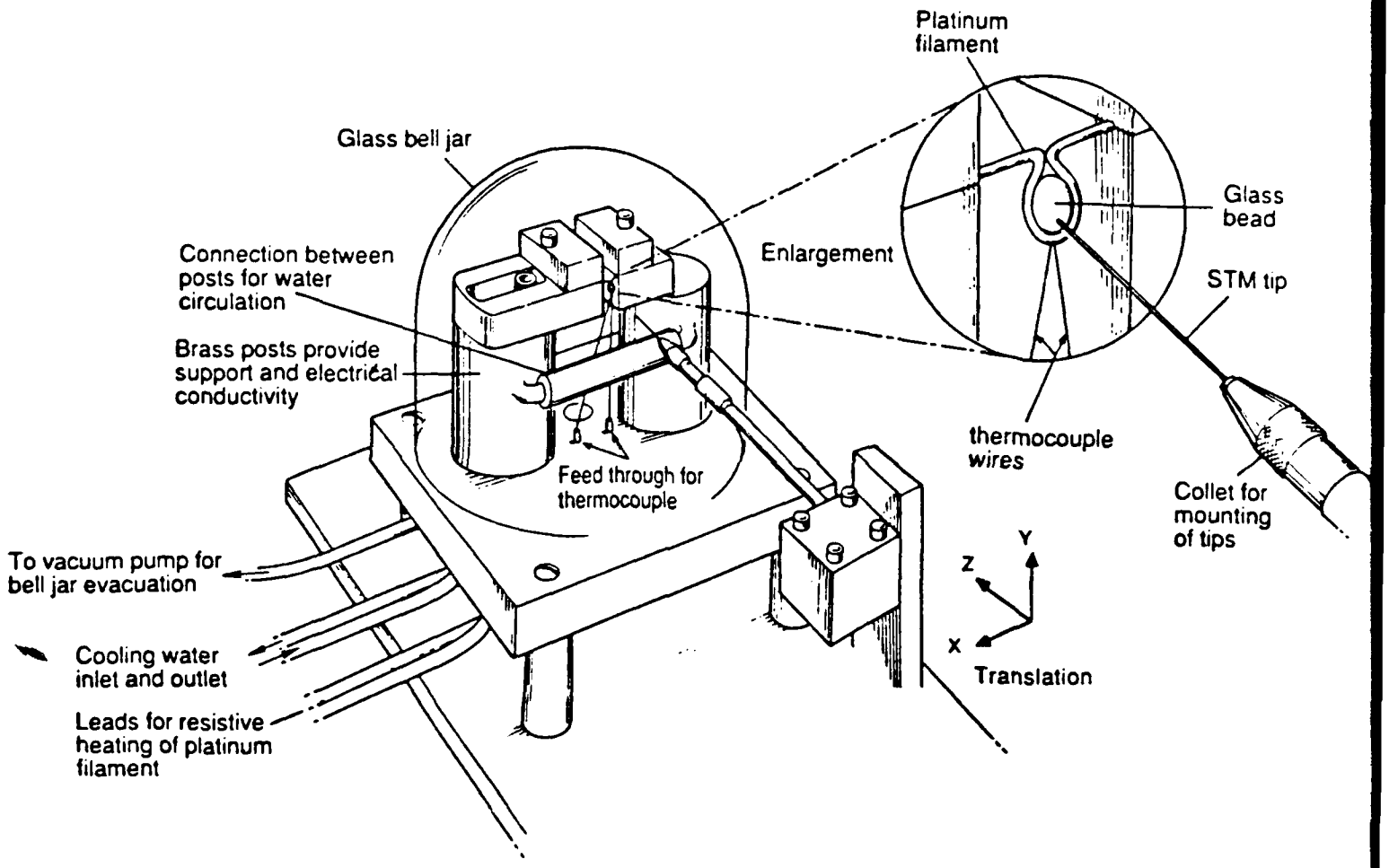
Platinum filament
Glass bell jar
Glass bead
Enlargement
Connection between posts for water circulation
STM tip
Brass posts provide support and electrical conductivity
thermocouple wires
Feed through for thermocouple
Collet for mounting of tips
To vacuum pump for bell jar evacuation
Y
Z
X
Translation
Cooling water inlet and outlet
Leads for resistive heating of platinum filament

Figure 1

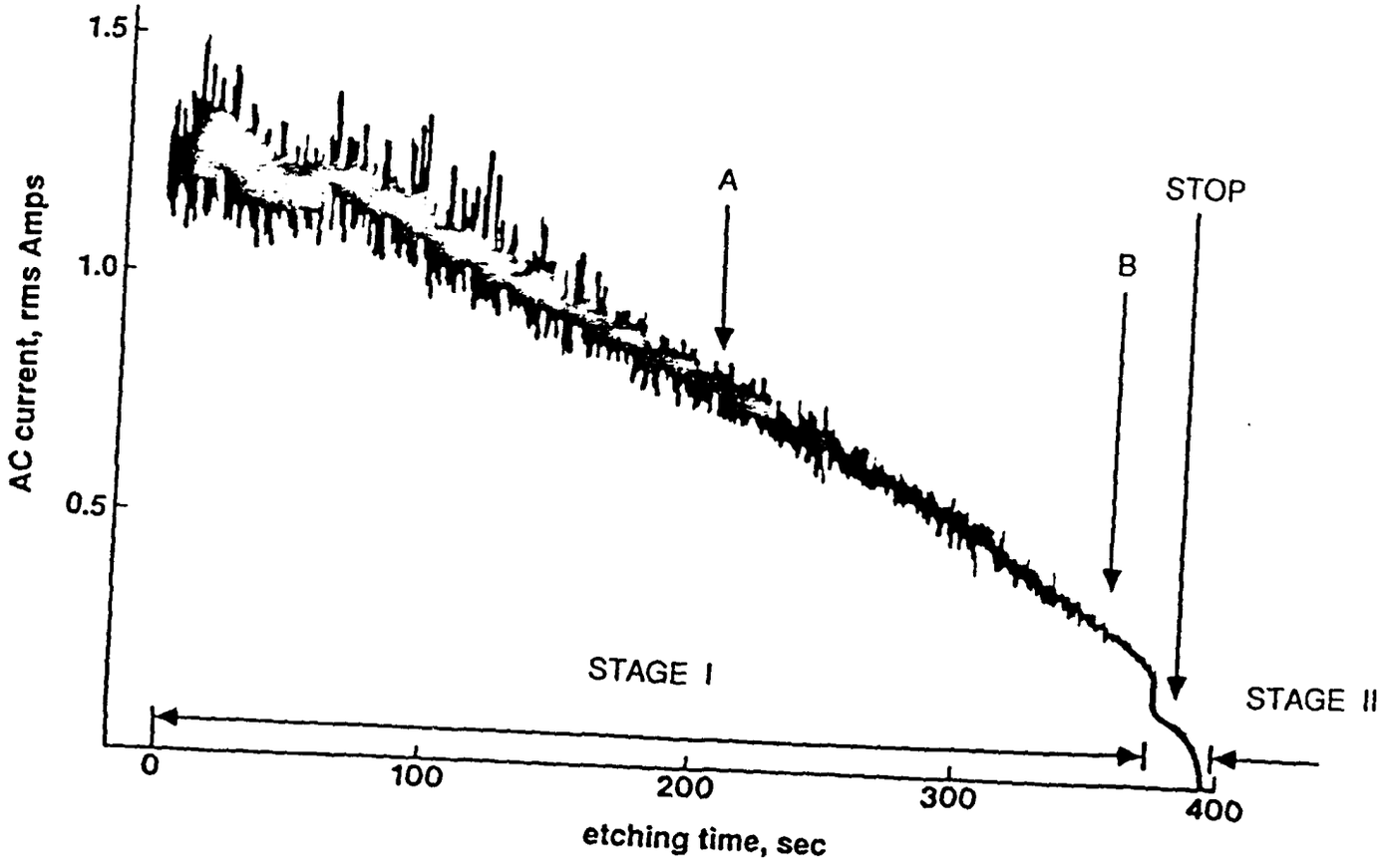
1.5
1.0
0.5
AC current, rms Amps
A
B
STOP
STAGE I
STAGE II
0
100
200
300
400
etching time, sec

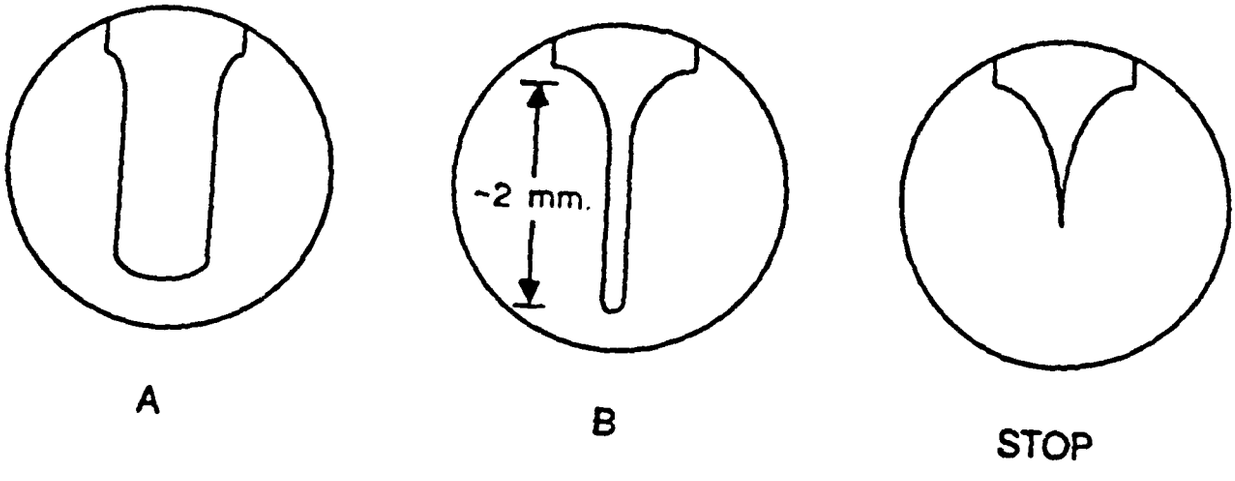
~2 mm.
A
B
STOP

Figure 2

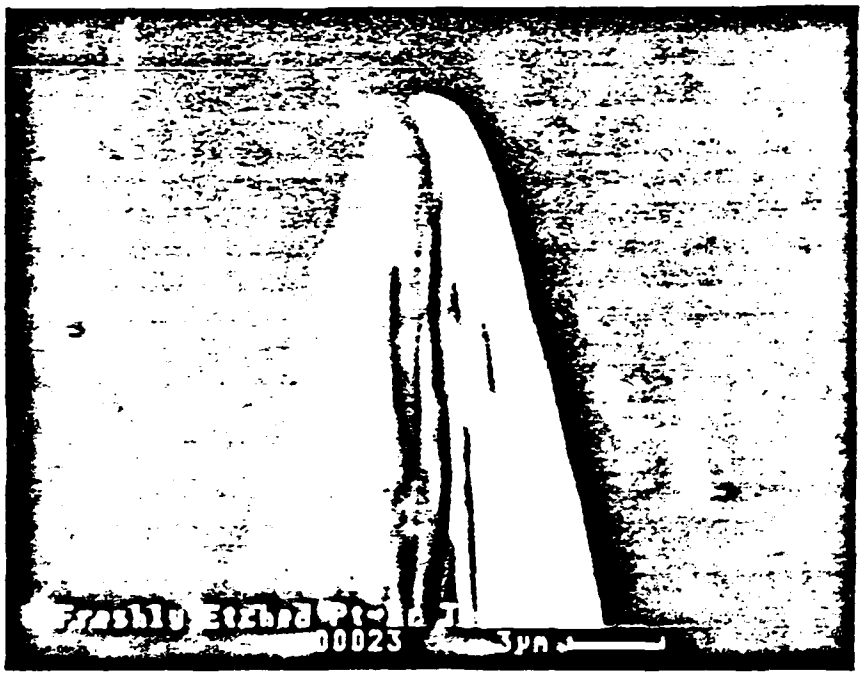

Figure 3

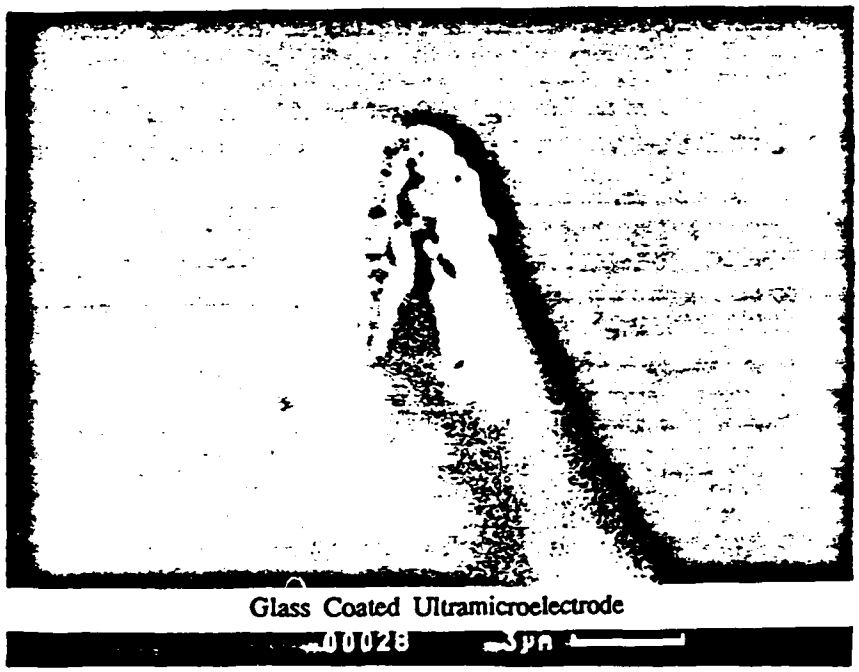

Figure 4a

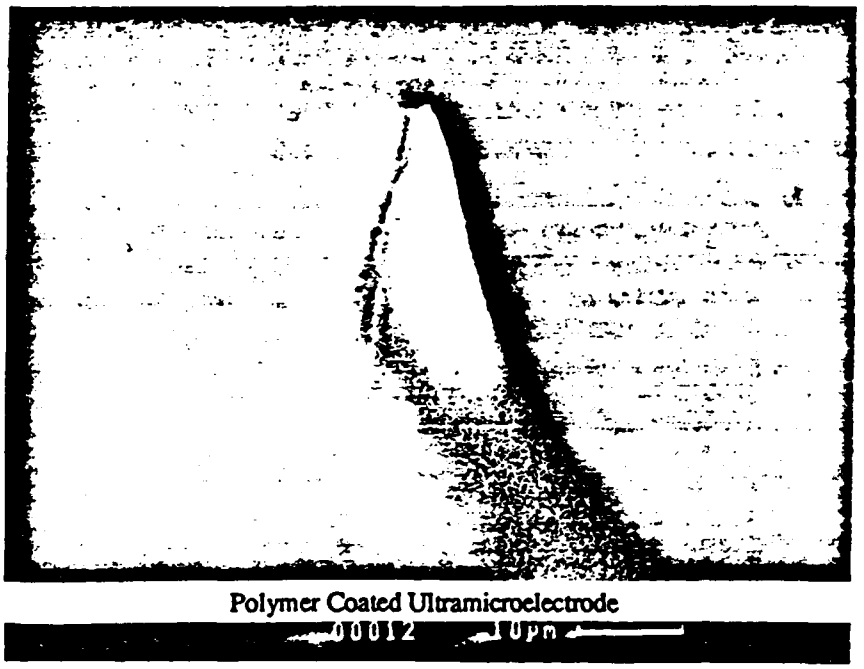

Figure 4b

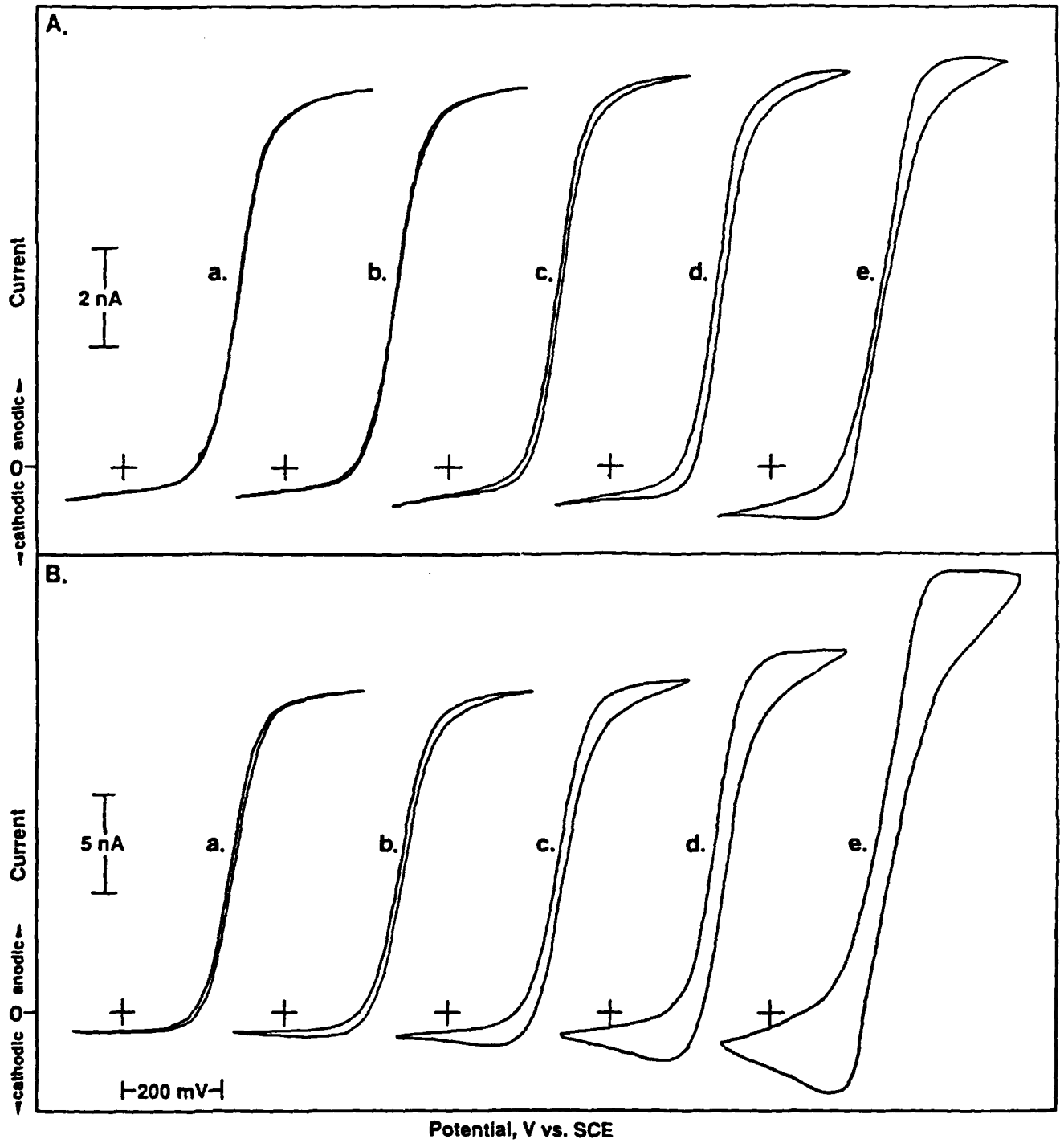
A.
2 nA
a.
b.
c.
d.
e.
Current
anodic
cathodic
O
B.
5 nA
a.
b.
c.
d.
e.
Current
anodic
cathodic
O
200 mV
Potential, V vs. SCE

Figure 5

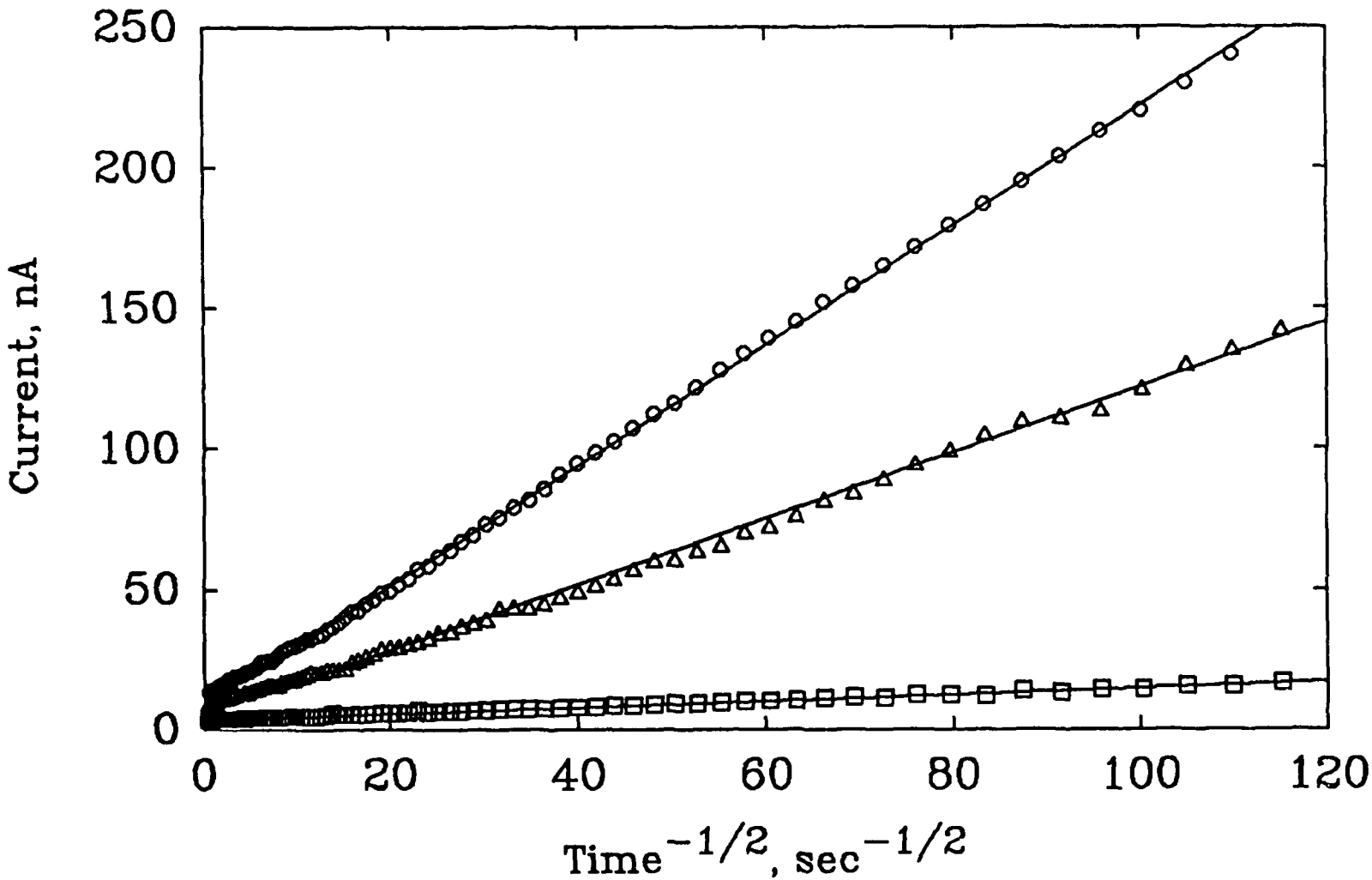
250
200
150
100
50
0
Current, nA
0
20
40
60
80
100
120
Time$^{-1/2}$, sec$^{-1/2}$

Figure 6a

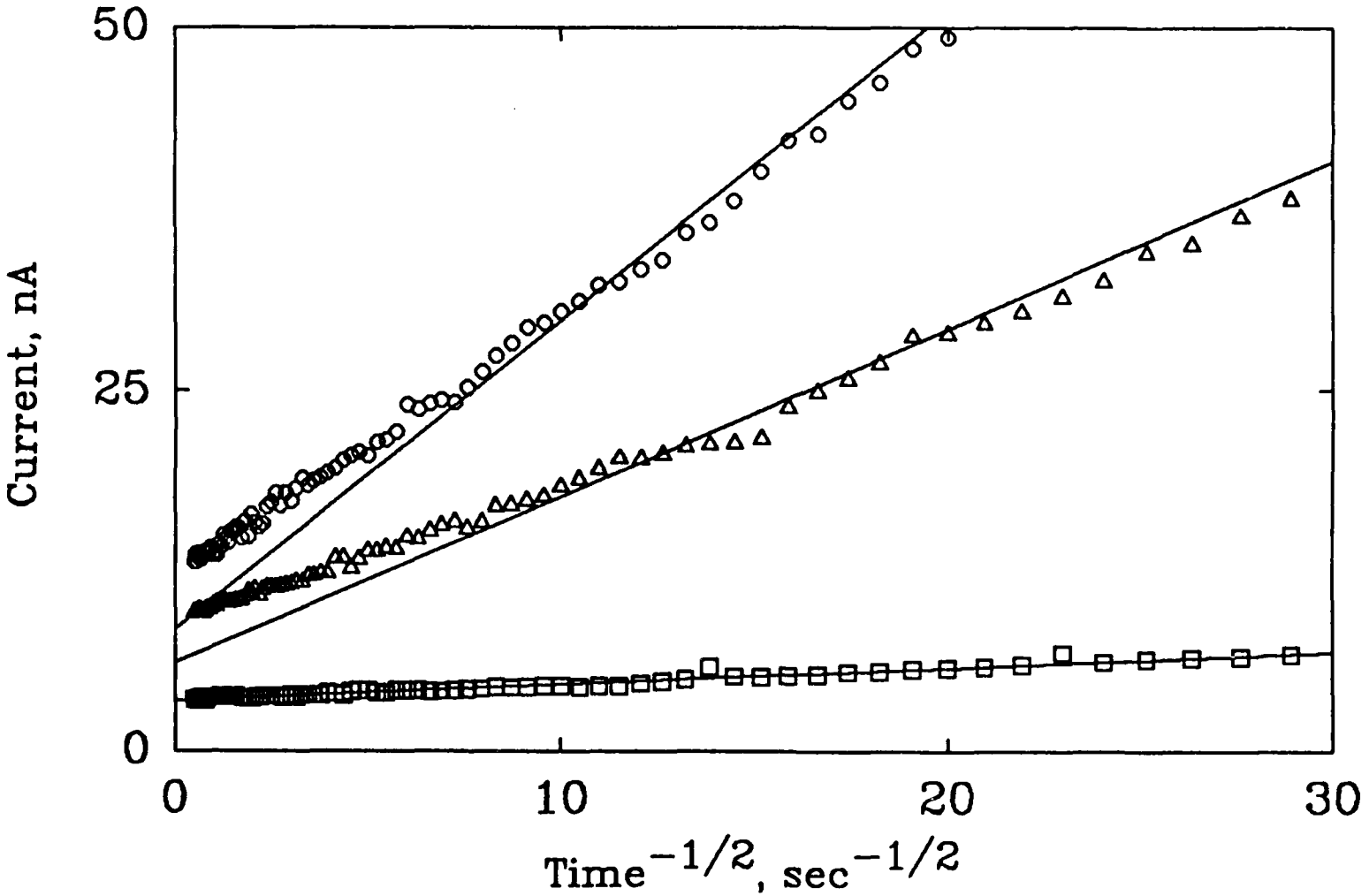

Figure 6b

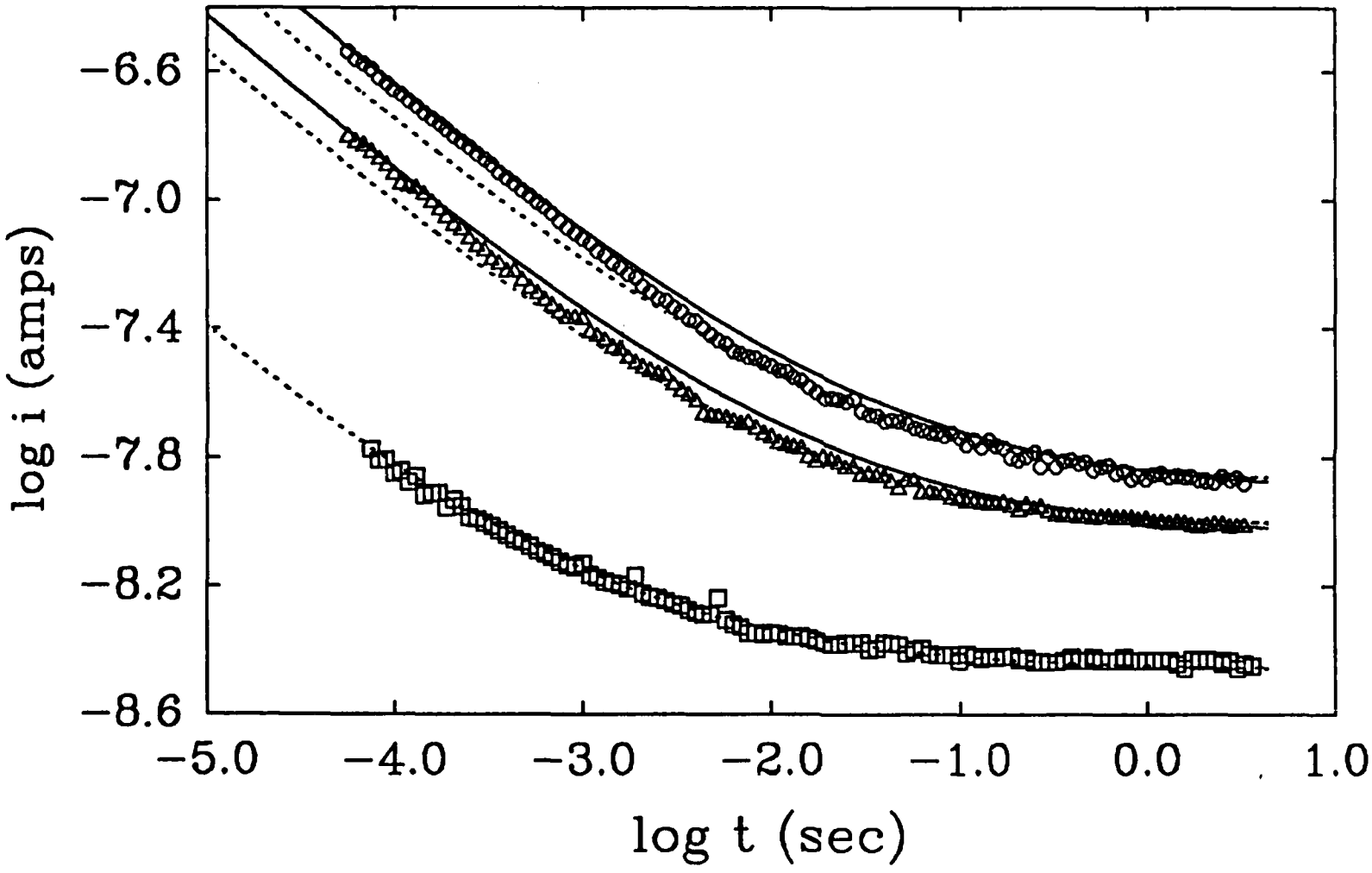

Figure 7

Scheme I

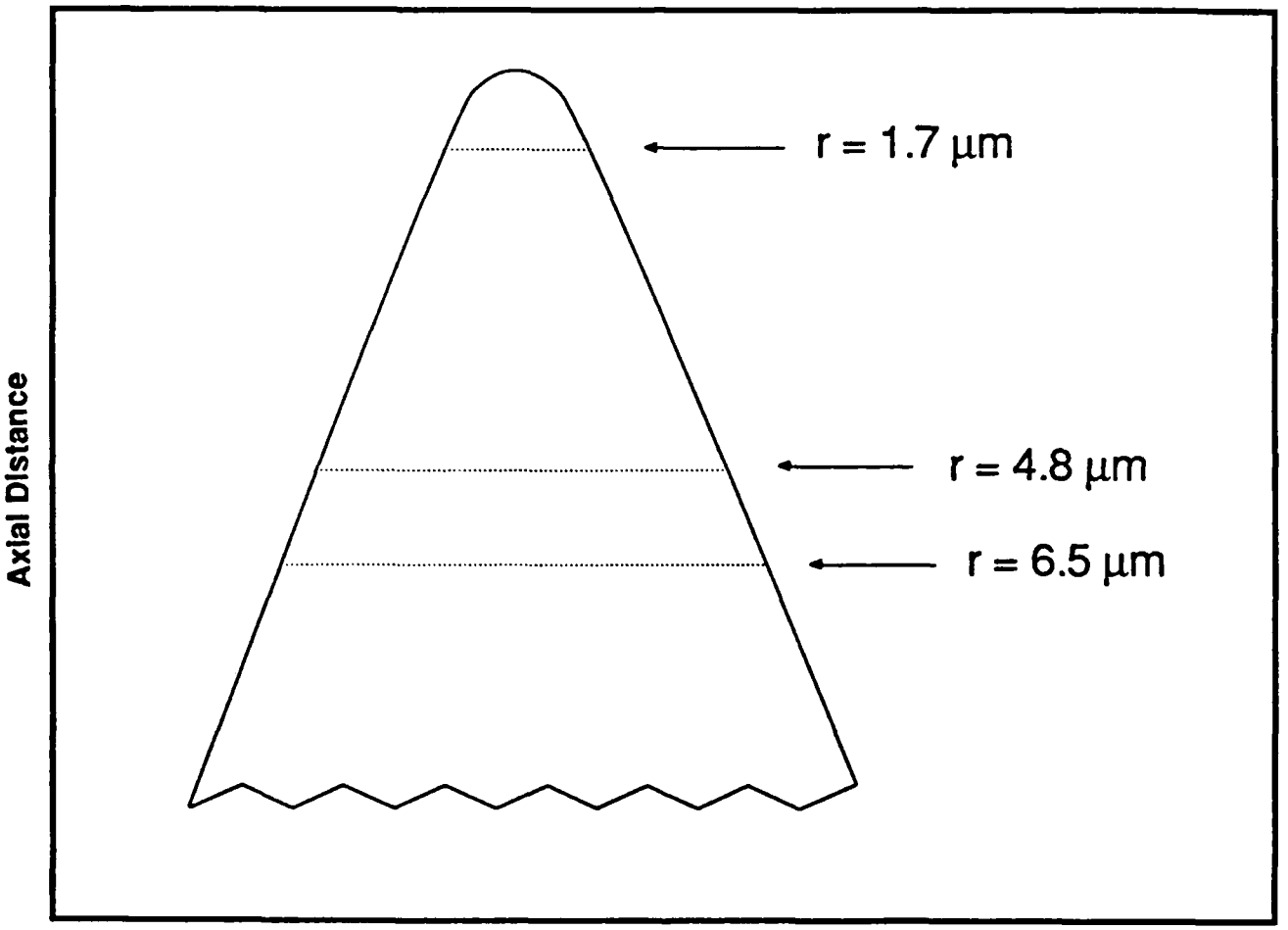

Scheme I